Seismic Performance Prediction of RC, BRB and SDOF Structures Using Deep Learning and the Intensity Measure I_{Np}

Omar Payán-Serrano [1], Edén Bojórquez [2,*], Julián Carrillo [3], Juan Bojórquez [2,*], Herian Leyva [4], Ali Rodríguez-Castellanos [2], Joel Carvajal [5] and José Torres [2]

[1] Department of Mechanical and Mechatronic Engineering (Metal-Mecánica), Tecnológico Nacional de México Campus Culiacán, Culiacan 80220, Mexico; omar.ps@culiacan.tecnm.mx

[2] Facultad de Ingeniería, Universidad Autónoma de Sinaloa, Culiacan 80013, Mexico; arodriguezca@uas.edu.mx (A.R.-C.); nacho.torres58@gmail.com (J.T.)

[3] Department of Civil Engineering, Universidad Militar Nueva Granada, UMNG, Bogota 110111, Colombia; julian.carrillo@unimilitar.edu.co

[4] Facultad de Ingeniería, Arquitectura y Diseño (FIAD), Universidad Autónoma de Baja California, Ensenada 22860, Mexico; herian.leyva@uabc.edu.mx

[5] Departamento de Física, Matemáticas e Ingeniería, Universidad de Sonora, Navojoa 85880, Mexico; joel.carvajal@unison.mx

* Correspondence: eden@uas.edu.mx (E.B.); juanbm@uas.edu.mx (J.B.)

Abstract: The motivation for using artificial neural networks in this study stems from their computational efficiency and ability to model complex, high-level abstractions. Deep learning models were utilized to predict the structural responses of reinforced concrete (RC) buildings subjected to earthquakes. For this aim, the dataset for training and evaluation was derived from complex computational dynamic analyses, which involved scaling real ground motion records at different intensity levels (spectral acceleration $Sa(T_1)$ and the recently proposed I_{Np}). The results, specifically the maximum interstory drifts, were characterized for the output neurons in terms of their corresponding statistical parameters: mean, median, and standard deviation; while two input variables (fundamental period and earthquake intensity) were used in the neural networks to represent buildings and seismic risk. To validate deep learning as a robust tool for seismic predesign and rapid estimation, a prediction model was developed to assess the seismic performance of a complex RC building with buckling restrained braces (RC-BRBs). Additionally, other deep learning models were explored to predict ductility and hysteretic energy in nonlinear single degree of freedom (SDOF) systems. The findings demonstrated that increasing the number of hidden layers generally reduces prediction error, although an excessive number can lead to overfitting.

Keywords: artificial neural networks; intensity measure; prediction model; maximum interstory drift; ductility; hysteretic energy

1. Introduction

Earthquake ground motions are a natural phenomenon that releases enormous amounts of energy; part of this energy is absorbed by bodies attached to the earth's surface. For this reason, earthquake ground motions put at risk the integrity and functionality of structures [1–4] as they have to dissipate an important part of the seismic energy. Due to the inherent properties of the construction materials, reinforced concrete buildings dissipate less energy than steel buildings [5–7]; thus, it is important to understand and predict the structural response or seismic performance of RC or RC-BRB buildings. Currently, some relevant studies have focused on presenting methods and mathematical expressions that assist in seismic design tasks using a relationship between ductility, μ, and period, T, to estimate important parameters or structural performance indices such as strength reduction factors and inelastic displacement ratios [8]; other studies have been dedicated to quantify

the risk seismic based on the structural damage [9,10] by selecting appropriate intensity measures [11–14].

1.1. Intensity Measures

The spectral acceleration at the first mode of vibration of the structure $Sa(T_1)$, where T_1 is the fundamental period, is considered the basic seismic intensity measure and, therefore, it is the most widely used parameter around the world [12]; however, new intensity measures based on the spectral shape parameter named N_p have been demonstrated to be useful in mathematical models for predicting important parameters of seismic performance, such as interstory drift and ductility of structures [13,15,16], especially the well-known I_{Np} intensity measure. According to Bojórquez and Iervolino [17], the I_{Np} intensity measure considers the nonlinear effects in the estimation of the structural response, and it has allowed scientists to obtain better results in comparison with most of the intensity measures presented in the literature [18]. The mathematical form of this parameter is $I_{Np} = Sa(T_1)N_p^\alpha$, where the spectral shape parameter N_p is obtained via Equation (1). In this equation, $Sa_{avg}(T_1 \dots T_N)$ represents the geometric mean of spectral acceleration in a range of periods.

$$N_p = \frac{Sa_{avg}(T_1, \dots, T_N)}{Sa(T_1)},$$

(1)

It is important to say that the information given by Equation (1) is that, if we have one or n records with a mean N_p value close to one, we can expect the average spectrum to be about flat in the period range between T_1 and T_N. For a mean N_p lower than one, an average spectrum with a negative slope is expected. Notice that the normalization of $Sa(T_1)$ lets N_p be independent of the scaling level of the records based on $Sa(T_1)$, but, most importantly, it helps to improve the knowledge of the path of the spectrum from period T_1 to T_N, which is related to the nonlinear structural response. On the other hand, α is a value determined from regression analysis. Several analyses of buildings under earthquakes developed by experts recommend a value for α of close to 0.4 [18] to predict peak interstory drift demands. The interstory drift is a relative displacement calculated by the difference between two consecutive floors, and it is the main parameter suggested by the seismic codes around the world to guarantee good structural performance. Moreover, the maximum interstory drift is a parameter of the structural response that allows for the determination of the seismic performance of a building [19]. Therefore, some experts have proposed methods to estimate this important indicator [13,20,21]; nevertheless, most of them are aimed to compute and predict interstory drifts based on traditional methods, and, currently, new techniques inspired by artificial intelligence approaches are in progress and represent the future for several engineering applications [22–28]. These efforts are focused on the prediction of the seismic performance of buildings by using novel ground motion intensity measures. In the present work, the computational tool of deep learning neural networks is used to predict the maximum interstory drift of reinforced concrete buildings under earthquakes. Moreover, the seismic performance of a complex building and several SDOF structures is tested via the neural network model and the advanced ground motion intensity measure I_{Np}.

1.2. Advances in Artificial Neural Networks

The computational advances at the end of the 20th century allowed for some mathematical models, proposed several years ago, to be a useful tool in resolving the basic problems of optimization, classification and prediction of response parameters [29–31]. The artificial neural networks are one of these models, which became known or classified as computational models. Nevertheless, they were limited in their ability to process data with a nature complex [32–34]. In the last decade, a type of neural network known as a deep learning network has dramatically improved prediction and classification results without human intervention to order and structure the data for the learning process [35–37].

1.3. Neural Networks in Civil Engineering

In the civil engineering field, several studies have utilized artificial neural networks to solve structural problems under dynamic loads of winds or earthquakes [38–42]; nevertheless, nowadays, there are not enough studies using deep learning networks to resolve problems with a high level of abstraction, as is the case of structural behavior. The computational models based on neural networks have greater potential for fitting data than traditional methods based on mathematical expressions. This is because, to a certain number of terms, a regression equation is impractical, while an artificial neural network does not become impractical as quickly due to an increased number of neurons or hidden layers. In addition, thanks to the continuous advancement of computer technology, computational models based on neural networks have shown that it is possible to obtain a high accuracy rate with relatively few data. For this reason, the first aim of this paper is to generate a computational model for the prediction of the seismic demand in terms of the maximum interstory drift of mid-rise RC structures under earthquake ground motions using deep learning networks and based on the two ground motion intensity measures $Sa(T_1)$ and I_{Np}. As a second objective, the neural network is tested by using a complex RC-BRB building. The third objective of the present study is to calibrate deep learning neural network models by means of several nonlinear SDOF systems with elastoplastic behavior subjected to the ground motion records but incorporating the ductility and normalized hysteretic energy as seismic performance parameters. Finally, Taylor diagrams are computed to illustrate the effectiveness of the prediction models in terms of statistical parameters.

2. Theoretical Framework

An artificial neural network (ANN) consists of a set of basic processing units called artificial neurons (Figure 1a) [43]. For an ANN, the connection of multiple neurons allows it to solve complex problems, which can be defined as linearly non-separable or nonlinear problems [44]. An arrangement of neurons in a reduced number of layers enables the solution of many problems only if the input data are properly categorized (Figure 1b), conversely, a drastic increase in the number of hidden layers helps to automatically resolve the classification of the data (Figure 2) [45]. This last type of ANN has proven to model high-level abstractions by applying multiple non-linear transformations.

The output of an artificial neuron is given by a function f known as the activation function which depends on the sum of the inputs $n_i w_i$ in the following way:

$$sum = 1w_0 + n_1 w_1 + n_2 w_2 + \cdots + n_i w_i, \tag{2}$$

where n_i is the output of another neuron and w_i is a value known as synaptic weight (Figure 1a). The value of the synaptic weight w_i determines the influence of the information that travels through the connection i. The sigmoid function allows to generate good approximations with normalized data between 0 to 1. The sigmoid function is mathematically expressed as follows:

$$f(sum) = n = \frac{1}{1 + e^{-sum}}, \tag{3}$$

where its derivate can be expressed by a simple form in terms of the same sigmoid function:

$$f'(sum) = d = n(1 - n). \tag{4}$$

The training process, also known as the learning process, of an ANN consists of defining, through iterations, the values of the synaptic weights, such as the prediction error decreases. The evaluation of the error at each iteration allows for the application of optimization techniques that update the values of the synaptic weights to obtain better performance. The Mean Square Error (MSE) function is a mathematical tool to quantify the error as follows:

$$E = MSE = \frac{1}{N} \sum_{i=1}^{N} (t_i - y_i)^2, \tag{5}$$

where N is the number of data points assigned to the training process, t_i is the target value for the prediction, and y_i is the output value of the ANN corresponding to the input i-th. The error can be described as a function that depends on the values assigned to the synaptic weights. In this way, the derivative of the error with respect to the synaptic weights describes the trend of the error in order to find a minimum. The quantification of the error trend is known as the gradient G and its mathematical expression is the following:

$$G = \frac{\partial E(w)}{\partial w},$$ (6)

where w is a vector that contains the values of the synaptic weights. The descending gradient method is an optimization approach that takes advantage of the information provided by the derivative of the error to adjust and update the values of the weights. The update of the weights to minimize the error would be given as follows:

$$w + \Delta w = w - \alpha G,$$ (7)

where Δw represents the update vector and α is a parameter, typically between 0 and 1, known as the learning rate, which determines the contribution of each iteration and controls how quickly the algorithm converges to a solution.
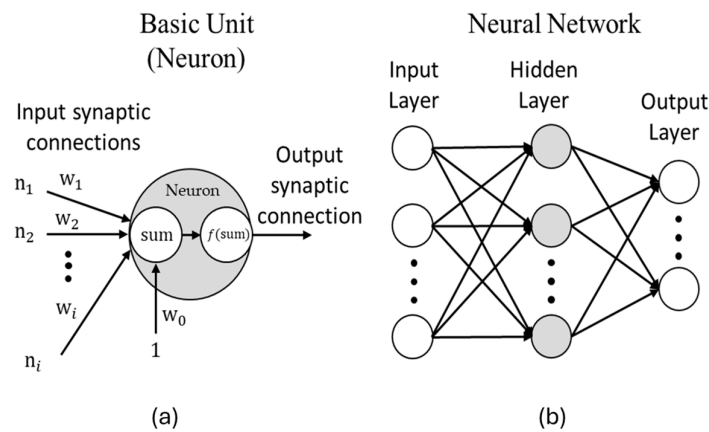

Figure 1. Artificial neural network: (**a**) internal neural process; (**b**) typical neural network.
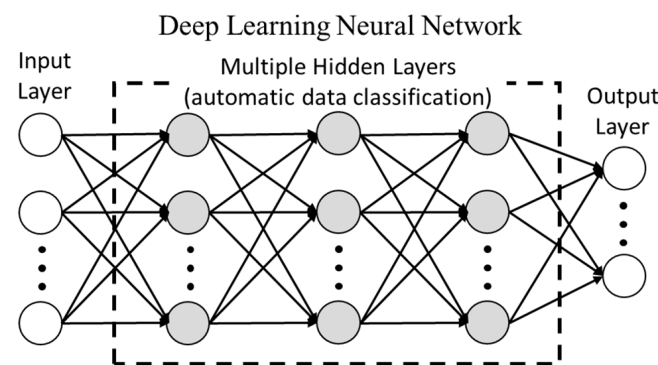

Figure 2. Deep neural network.

3. Methodology

To generate an acceptable prediction model, it is necessary to have a considerable amount of data that allows for an accurate description of the behavior of the variable of interest. For this work, the data necessary to describe the behavior of the maximum interstory drift of RC mid-rise frames under earthquake ground motions are shown in Figures 3 and 4. These data were obtained by incremental dynamic analysis [46] using

registered records of earthquake ground motions which are scaled at different spectral acceleration $Sa(T_1)$ and I_{Np} values. Notice that a total of 2400 nonlinear seismic analyses of RC structures have been performed. The ground motion records correspond to seismic events with magnitudes close to seven or higher, and an epicenter located at 300 km or more from Mexico City. The most important structural damage by seismic events in Mexico has occurred in the area selected for the extraction of records. This area is known as the Lake Zone, which has been characterized by soil periods between 2 and 3 s; therefore, the peak ground acceleration PGA and velocity PGV can produce high levels of shaking in buildings. More information about the characteristics of the seismic records and of the buildings is presented in Tables 1 and 2, respectively, while Figure 5 illustrates the structural configuration of the RC frames. In addition, several details about the structural elements (beams and columns) used in the study buildings are shown in Figure 6 and Table 3. In Figure 6, the cross-section and the configuration of the reinforcing steel area are described. It is important to say that all the structural buildings used for the present study have been designed according to the Mexico City Building Code.
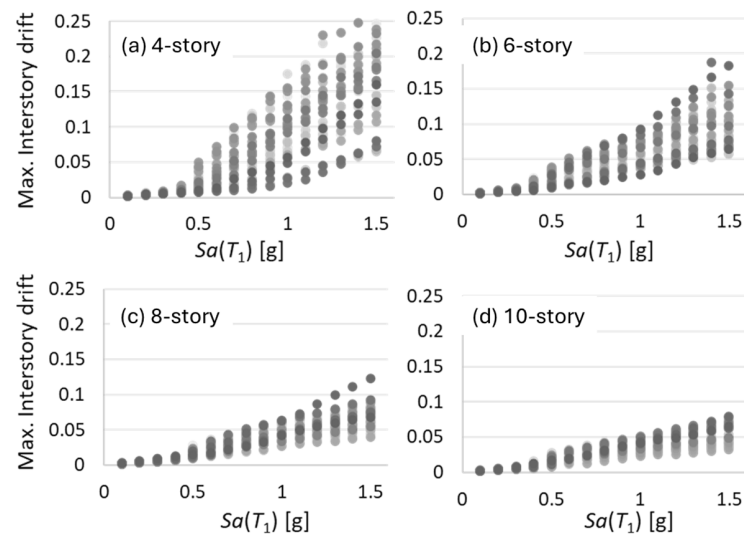

Figure 3. Maximum interstory drift using spectral acceleration $Sa(T_1)$ for mid-rise buildings with (**a**) 4 stories; (**b**) 6 stories; (**c**) 8 stories; (**d**) 10 stories.
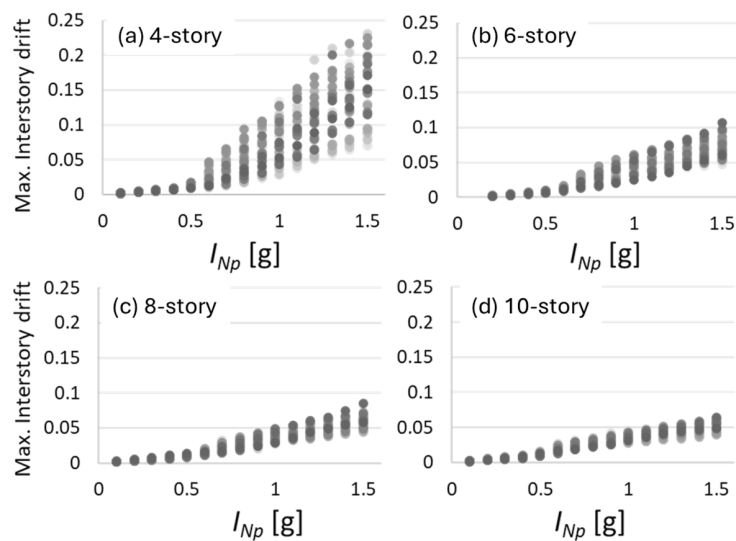

Figure 4. Maximum interstory drift using the spectral shape I_{Np} for mid-rise buildings with (**a**) 4 stories; (**b**) 6 stories; (**c**) 8 stories; (**d**) 10 stories.

Table 1. Earthquake ground motions.

Record	Magnitude	PGV [cm/s]	PGA [cm/s^2]	Date	Station
1	8.1	59.5	178.0	19 September 1985	SCT
2	7.6	14.6	48.7	21 September 1985	Tlahuac deportivo
3	6.9	15.6	45.0	25 April 1989	Alameda
4	6.9	21.5	68.0	25 April 1989	Garibaldi
5	6.9	12.8	44.9	25 April 1989	SCT
6	6.9	15.3	45.1	25 April 1989	Sector Popular
7	6.9	17.3	52.9	25 April 1989	Tlatelolco TL08
8	6.9	17.3	49.5	25 April 1989	Tlatelolco TL55
9	7.3	12.2	39.3	14 April 1995	Alameda
10	7.3	10.6	39.1	14 September 1995	Garibaldi
11	7.3	9.62	30.1	14 September 1995	Liconsa
12	7.3	9.37	33.5	14 September 1995	Plutarco Elías Calles
13	7.3	12.5	34.3	14 September 1995	S. Popular
14	7.3	7.8	27.5	14 September 1995	Tlatelolco TL08
15	7.3	7.4	27.2	14 September 1995	Tlatelolco TL55
16	7.5	4.6	14.4	9 October 1995	Cibeles
17	7.5	5.1	15.8	9 October 1995	CU Juárez
18	7.5	4.8	15.7	9 October 1995	C. urbano P Juárez
19	7.5	8.6	24.9	9 October 1995	Córdoba
20	7.5	6.3	17.6	9 October 1995	Liverpool
21	7.5	7.9	19.2	9 October 1995	Plutarco Elías Calles
22	7.5	5.3	13.7	9 October 1995	S. Popular
23	7.5	7.18	17.9	9 October 1995	V. Gómez
24	6.9	5.9	16.2	11 January 1997	CU Juárez
25	6.9	5.5	16.3	11 January 1997	C. urbano P Juárez
26	6.9	6.9	18.7	11 January 1997	García Campillo
27	6.9	8.6	22.2	11 January 1997	Plutarco Elías Calles
28	6.9	7.76	21.0	11 January 1997	10 Roma A
29	6.9	7.1	20.4	11 January 1997	11 Roma B
30	6.9	7.2	16.0	11 January 1997	Tlatelolco TL08

Table 2. Characteristics of RC frame models.

Frame ID	Number of Stories	Period of Vibration (s)	
		T$_1$	T$_2$
F4	4	0.90	0.31
F6	6	1.20	0.39
F8	8	1.38	0.44
F10	10	1.53	0.48

Table 3. Characteristics of RC beams and columns in cm or cm^2.

Element ID_Frame(Story Loc)	Characteristic	F4	F6	F8	F10
Beam 1 F4(1–2) F6(1–3) F8(1–3) F10(1–4)	B	25	25	35	35
	H	55	60	80	90
	As_sup	12.7	19.1	47.7	56.2
	As_inf	7.6	13.2	38.9	47.9
	spacing_ext	15	15	15	10
	spacing_cen	25	25	15	10
Beam 2 F4(3–4) F6(4–6) F8(4–6) F10(5–7)	B	20	20	35	35
	H	50	55	70	75
	As_sup	9.5	13.8	39.5	47.3
	As_inf	4.4	7.8	27.2	37.6
	spacing_ext	15	15	15	10
	spacing_cen	25	25	20	15

Table 3. *Cont.*

Element ID_Frame(Story Loc)	Characteristic	F4	F6	F8	F10
Beam 3 F8(7–8) F10(8–10)	B			30	35
	H			55	65
	As_sup			22.6	27.3
	As_inf			10	15.2
	spacing_ext			15	15
	spacing_cen			25	25
Column 1 F4(1–2) F6(1–3) F8(1–3)	B	50	60	95	110
	H	50	60	95	110
	As	64.39	95.89	190.25	242.29
	Spacing	15	10	10	10
Column 2 F4(3–4) F6(4–6) F8(4–6)	B	40	50	85	100
	H	40	50	85	100
	As	45.19	49.12	72.25	100
	Spacing	10	15	15	15
Column 3 F8(7–8)	B			75	90
	H			75	90
	As			56.25	81
	spacing			15	15

Table 3 defines the most important characteristics, such as height (H), width (B), superior steel area (As_sup), inferior steel area (As_inf), spacing of stirrups in the extremes (spacing_ext), and spacing of stirrups in the center (spacing_cen). Notice that the units of Table 3 are provided in centimeters (cm) or square centimeters (cm^2).

For ANN-based computational models, it is considered good practice to normalize the data using different scales and ranges. Although the model could converge without the normalization of the characteristics, the resulting model will be dependent on the choice of the units used in the input. To normalize the values in the range [0, 1], the following mathematical expression was used:

$$\overline{x}_i = \frac{x_i - x_{min}}{x_{max} - x_{min}}, \tag{8}$$

where $\overline{x}_i$ is the normalized value, x_i is the value to normalize, x_{min} is the minimum value, and x_{max} is the maximum value. Following the guidelines of good practice for the generation of models based on neural networks, the next stage is to partition the data. The separation of the data is carried out randomly under the following criteria: 70% for training and 30% for validating. The validation data are used to improve the evaluation of the model fit during the training process while the optimizer is running. The optimizer applied was the ADAM algorithm with MSE of loss function and a learning rate of 0.001 [47]. A small learning rate slows down the learning process but converges smoothly, while a large learning rate speeds up the learning but may not converge. Generally, a small learning rate is preferred. This optimizer method is based on the gradient descent approach, and, according to Kingma and Ba, the method is computationally efficient and is well suited for problems that are large in terms of data or parameters [47]. Furthermore, the MSE function is one of the most frequent loss functions used due to its continuity characteristic, which is very important when optimizers based on the descending gradient approach are used. This practice allows us to analyze the performance of the ANN due to unknown data which are not used for processing the network learning. In addition, the problem known as over-fitting can be determined with the help of an error behavior study. This problem appears when the neural network architecture is very complex for the purpose of simple tasks or when the interactive process of learning is too long [48].
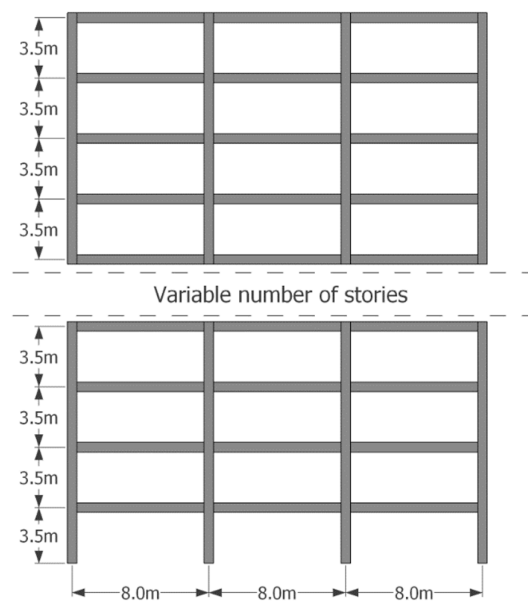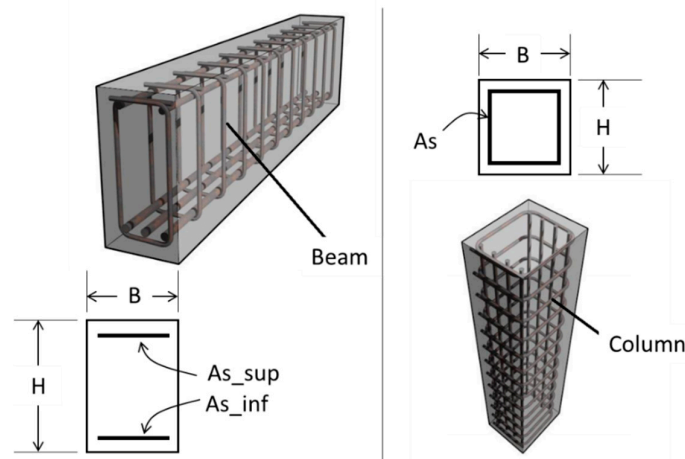
Figure 5. RC frame configuration.

Figure 6. RC beams and columns configuration.

4. Numerical Results

For the design of the architecture and the training process of the neural networks, the fundamental period and the ground motion intensity measure are the input variables, while the mean, median, and standard deviation of the maximum interstory drift are the output variables. Figure 7 shows the generic neural network architecture with multi-hidden layers, two neuron inputs, and tree neuron output. The input variables describe, in very general terms, the characteristics of the problems, because the fundamental period is one of the most important structural characteristics, and the seismic intensity measure describes the earthquake hazard using a simple value. Other seismic and structural features could be used as inputs to simplify the learning process; however, the deep neural network approach suggests modeling complex data using few inputs from multiple hidden layers between the input and output layers, hence the name "deep" networks. The output variables correspond to statistical parameters, which characterize, in general terms, the behavior of the maximum interstory response of RC mid-rise buildings under earthquake ground motions (Figures 8 and 9). The mean and median are two statistical measures of central tendency that can be used to identify potential skewness in the distribution of data; that is, if the difference between the mean and median is high, it means that the data tend towards higher or lower values. The dataset of Figure 9 is in Appendix A.
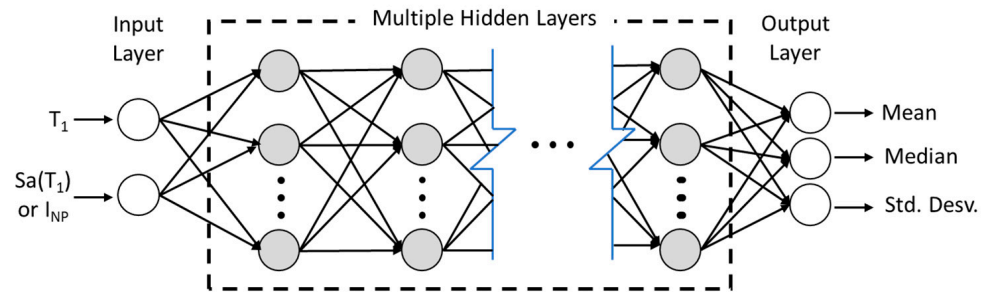
Figure 7. General configuration of deep neural networks to estimate the mean, median, and standard deviation.
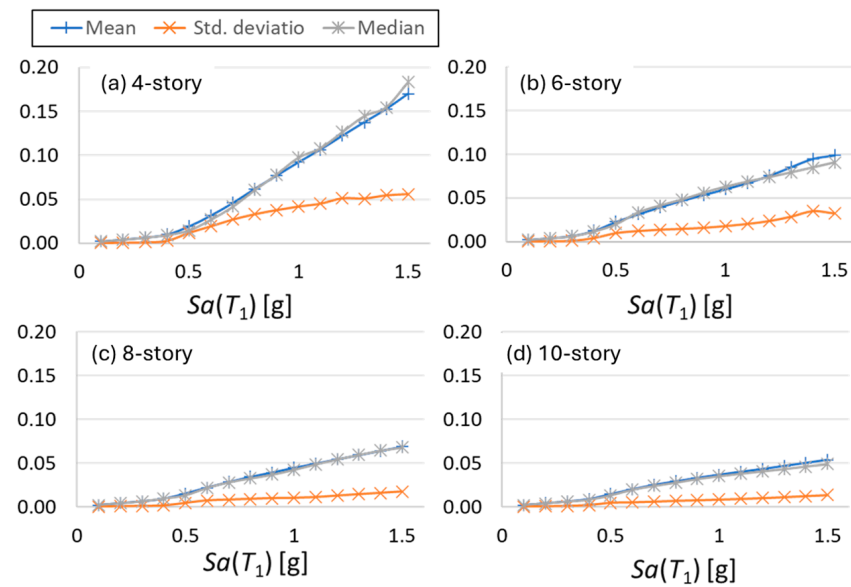

Figure 8. Mean, median, and standard deviation of the maximum interstory drift using spectral acceleration $Sa(T_1)$ for mid-rise with (**a**) 4 stories; (**b**) 6 stories; (**c**) 8 stories; (**d**) 10 stories.
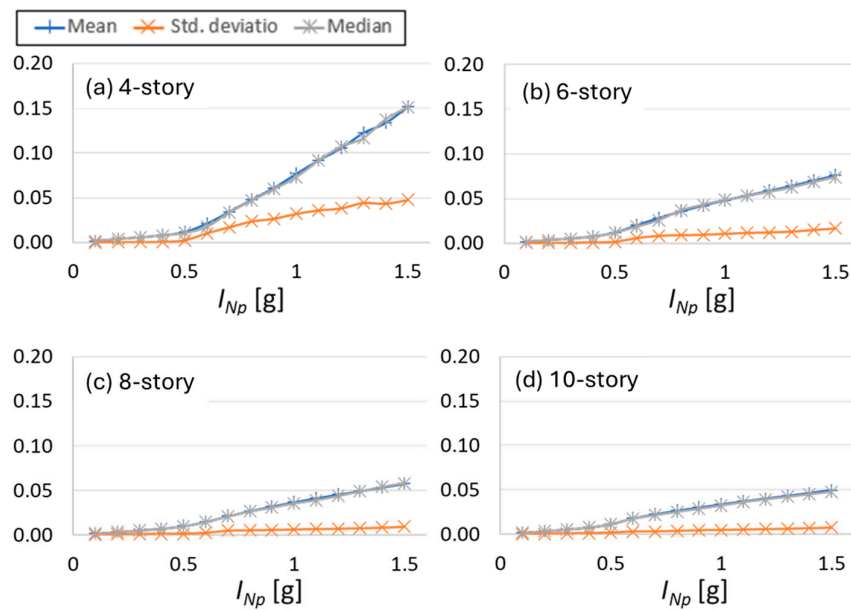

Figure 9. Mean, median, and standard deviation of the maximum interstory drift using the spectral shape I_{Np} for mid-rise with: (**a**) 4 stories; (**b**) 6 stories; (**c**) 8 stories; (**d**) 10 stories.

A correlation analysis between the input and output variables is presented in Figure 10. The mean, median, and standard deviation (outputs) have a moderate to significant or strong relationship with respect to the fundamental period and the intensity measure (inputs). Notice that, in Figure 10, no relationship between the input variables is observed, therefore, they were used as input neurons for the ANN model.
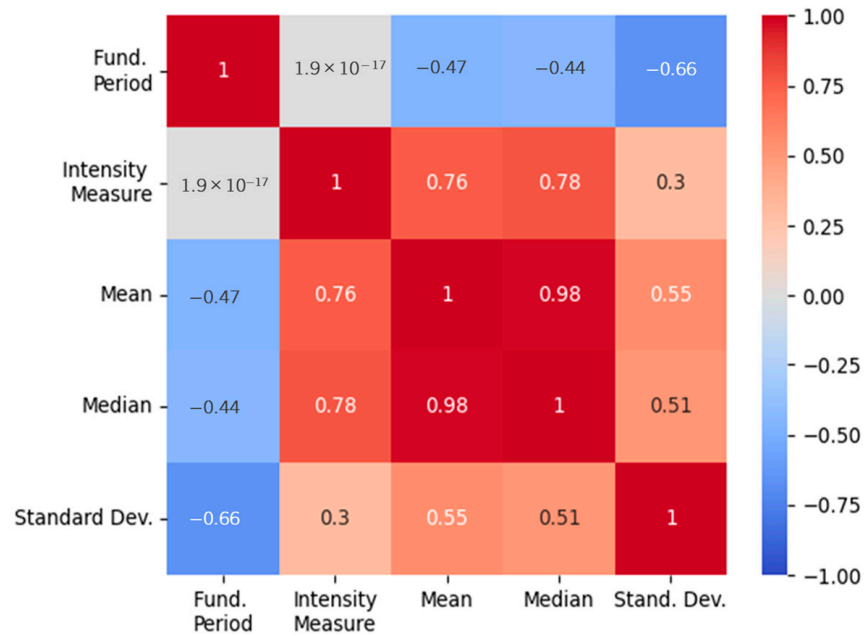

Figure 10. Correlation matrix between input and output variables.

The number of neurons in the input layer and the output layer are directly defined by the problem to solve, while the selection of the optimal number of hidden layers and their neurons is not directly determined. For this reason, it is necessary to study different configurations of hidden layers. Thanks to the multiple hidden layers, a deep neural network can solve complex regression or non-linear classification problems, however, with many hidden neurons it is possible to reach overlearning more quickly [49]. Therefore, a pyramid-shaped architecture is adopted to mitigate this common problem pertinent to deep network models. Table 4 summarizes the neural network configurations and their performance in the task of prediction. The configuration [2, 3, 3] indicates an array with 2 input neurons, 3 neurons in a hidden layer, and 3 output neurons, while the configuration [2, 10, 7, 3] represents a neural architecture with 2 input neurons, 10 neurons in the first hidden layer, 7 neurons in the second hidden layer, and 3 output neurons. Numerically, Table 4 shows the decrease in the error when the number of hidden layers increases.

Table 4. Results of the training process to predict statistics of the interstory drift.

Neurons Configuration	Hidden Layers	Training Data	Evaluation Data	Training Iterations	MSE Training Data	R^2 Training Data	MSE Evaluation Data	R^2 Evaluation Data
[2, 3, 3]	1	70%	30%	5000	0.00538	0.75	0.00832	0.65
[2, 6, 3]	1	70%	30%	5000	0.00284	0.77	0.00350	0.76
[2, 12, 3]	1	70%	30%	5000	0.00262	0.78	0.00304	0.76
[2, 10, 7, 3]	2	70%	30%	5000	0.00093	0.81	0.00120	0.80
[2, 15, 9, 5, 3]	3	70%	30%	5000	0.00062	0.93	0.00084	0.85
[2, 15, 10, 7, 5, 3]	4	70%	30%	5000	0.00036	0.95	0.00053	0.94
[2, 15, 11, 9, 7, 5, 3]	5	70%	30%	5000	0.00016	0.98	0.00145	0.79

The training error and evaluation error of neural networks with 1, 2, 3, 4, and 5 hidden layers are shown in Figure 11. Graphically, it is possible to observe the behavior of the errors and detect possible problems of over-fitting. The training error is drastically reduced by increasing a hidden second layer. However, from five hidden layers, the over-fitting problem starts to appear significantly. The neural network with four hidden layers of neural configuration [2, 15, 10, 7, 5, 3] offers a good prediction with training data or evaluation data.
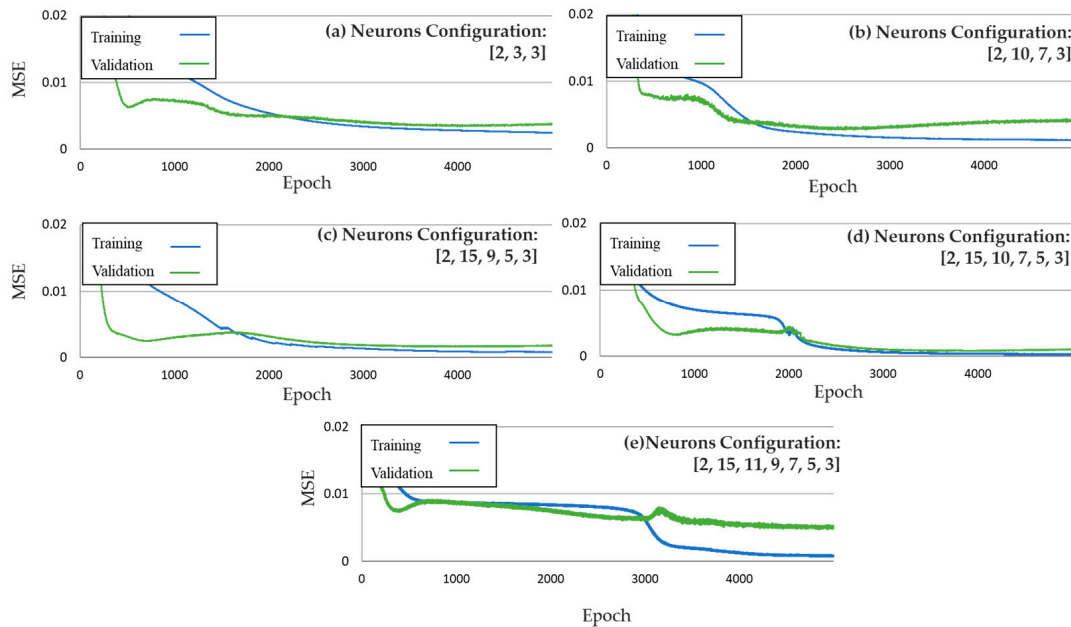
Figure 11. Error behavior due to a neural configuration: (**a**) [2, 3, 3]; (**b**) [2, 10, 7, 3]; (**c**) [2, 15, 9, 5, 3]; (**d**) [2, 15, 10, 7, 5, 3]; (**e**) [2, 15, 11, 9, 7, 5, 3].

A correlation graph between the target value and the response of the neural network allows us to visualize the degree of dispersion. Several correlation graphs are introduced in Figure 12 to show the degree of approximation offered by some of the neural configurations. The neural network with one hidden layer presents great drawbacks in describing each one of the outputs. With two hidden layers, the problem of describing some of the three output variables is solved; however, the standard deviation is not well correlated. From four hidden layers, all output variables are adjusted to acceptable correlation values. While more layers can help to improve this fit and decrease dispersion, the problem of overfitting would become significant.

To validate the results of the neural configuration [2, 15, 10, 7, 5, 3], Table 5 shows the results of the application of the technique known as cross-validation. This technique allows us to observe the independent degree of the error with respect to the data selected for the training process [50]. A minimum variation of the error of each training process indicates that the magnitude of this error is independent of the randomly selected data, while a significant variation indicates that the random selection of data for the training process influences the degree of prediction of the neural network. The error variation for neural configuration with four hidden layers is minimal; therefore, the amount of data generated to describe the behavior of the output variables is adequate. In this way, the random selection of the data corresponding to the partition of the training process is independent of the efficiency achieved by the neural networks.
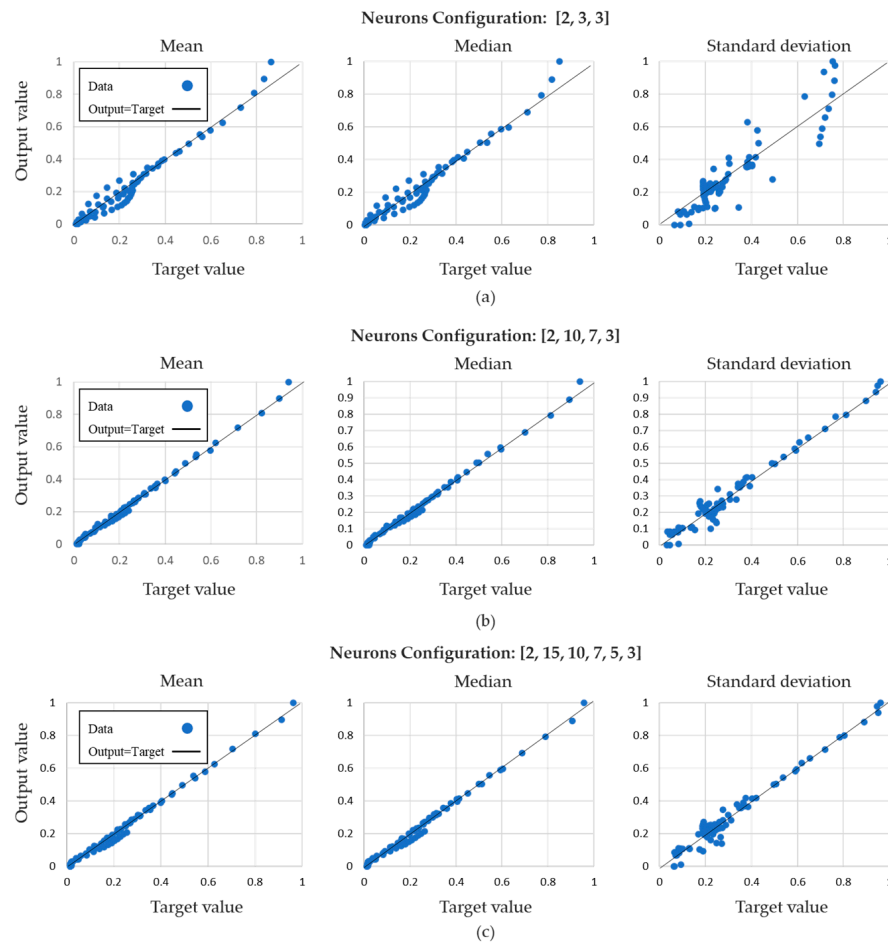
Figure 12. Relations between target values and output values due to a neural configuration: (**a**) [2, 3, 3]; (**b**) [2, 10, 7, 3]; (**c**) [2, 15, 10, 7, 5, 3].

Table 5. Cross-validation for [2, 15, 10, 7, 5, 3].

Training ID	MSE Training Data	MSE Evaluation Data
1	0.0002450	0.0002520
2	0.0002145	0.0002235
3	0.0002320	0.0002420
4	0.0002214	0.0002315
5	0.0002351	0.0002452
6	0.0002170	0.0002260
7	0.0002443	0.0002533
8	0.0002246	0.0002335
9	0.0002330	0.0002410
10	0.0002302	0.0002413

A graphic representation of the prediction performance of different models can be given from the well-known Taylor diagram, which is a visual aid to analyze and compare models from its three statistics attained: correlation coefficient, the root-mean-square error (RMSE), and the standard deviation [51]. Figure 13 shows a Taylor diagram with the prediction models of one, two, and four hidden layers. The brown circular dashed lines around the blue star (ideal prediction model) represent the error. The model with four hidden layers is the closest to the blue star; therefore, this model could be announced as the most accurate model because it has less error, higher correlation, and similar deviation.
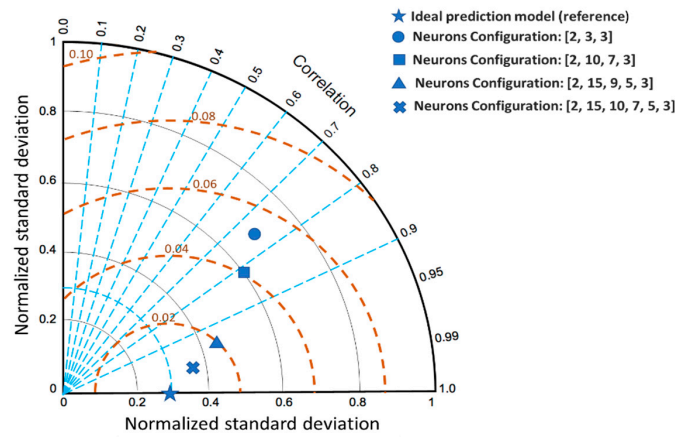
Figure 13. Taylor diagram of models to predict statistics of the interstory drift.

5. Deep Learning Model Tested to Assess the Seismic Performance of a Complex RC-BRB Building

This chapter focuses on assessing the performance of deep learning neural networks in predicting the maximum interstory drift of an RC-BRB. In order to test the deep learning model presented in Chapter 4, a nine-story RC-BRB building is evaluated. The main characteristics of the structural model are shown in Table 6, and Figure 14 illustrates a 3D view of the braced building with 9 stories. Notice that all the buildings were designed under seismic loads corresponding to the Mexico City Building code. It was proposed to use a different section of beam and column for each 3 floors, and one BRB section for the framed building. Table 7 shows the sections and the main properties of the structural model obtained.

Table 6. Main geometric characteristics from designed model.

Model	Number of Floors	Bays Dir. X	Bays Dir. Y	Interstory Height (m)	Bays Length (m)
RC9-BRB	9	3	3	3.5	7

Table 7. Main properties of the nine RC-BRB building model (dimensions in cms).

Model Property	RC9-BRB
Column1	60x60
Column2	45x45
Column3	35x35
Beam1	30x55
Beam2	30x60
Beam3	25x50
BRB	36
Cy	0.45
Period (s)	0.87

The RC-BRB building with nine stories was subjected to the ground motion earthquakes of Table 1 in order to compute incremental dynamic analysis at different intensity levels in terms of I_{Np} and maximum interstory drift. Figure 15a illustrates the results of the incremental dynamic analysis and the corresponding values of the maximum interstory drift, while Figure 15b shows the performance of the trained neural network. It is observed that the network allows close values to be obtained for the complex incremental dynamic analysis results. It is important to say that a coefficient of determination (R^2) of 95% was obtained in such a way that the deep neural network could be a good tool for seismic pre-design tasks and the fast estimation of the structural response or performance of buildings under earthquakes.
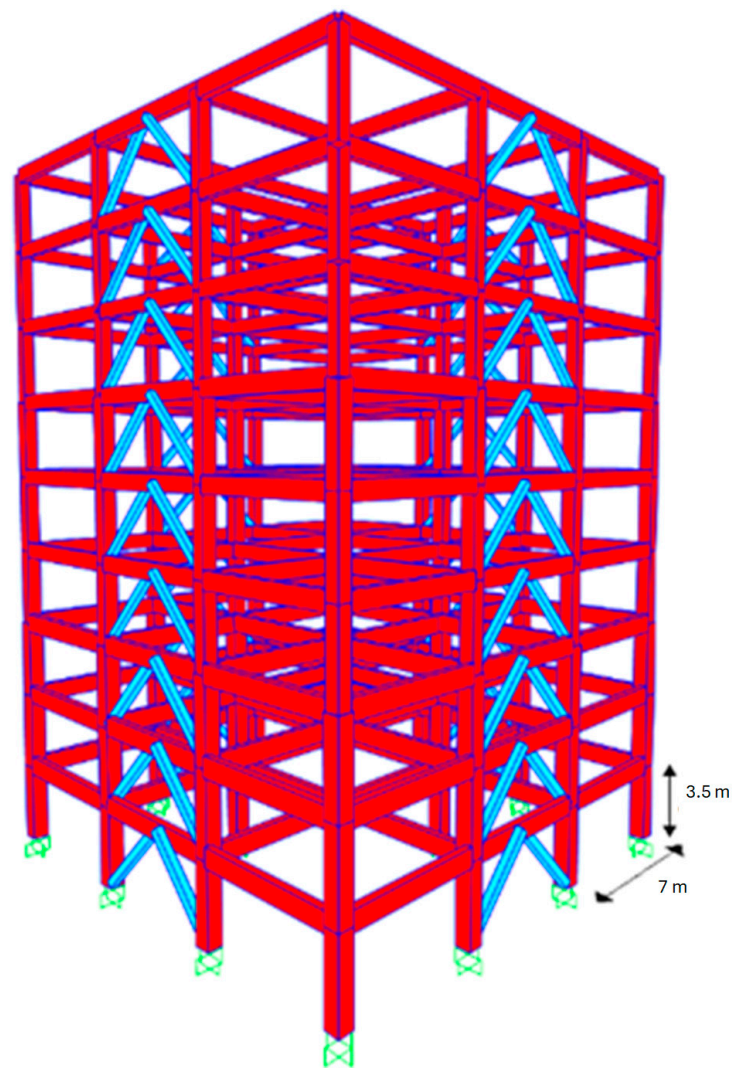
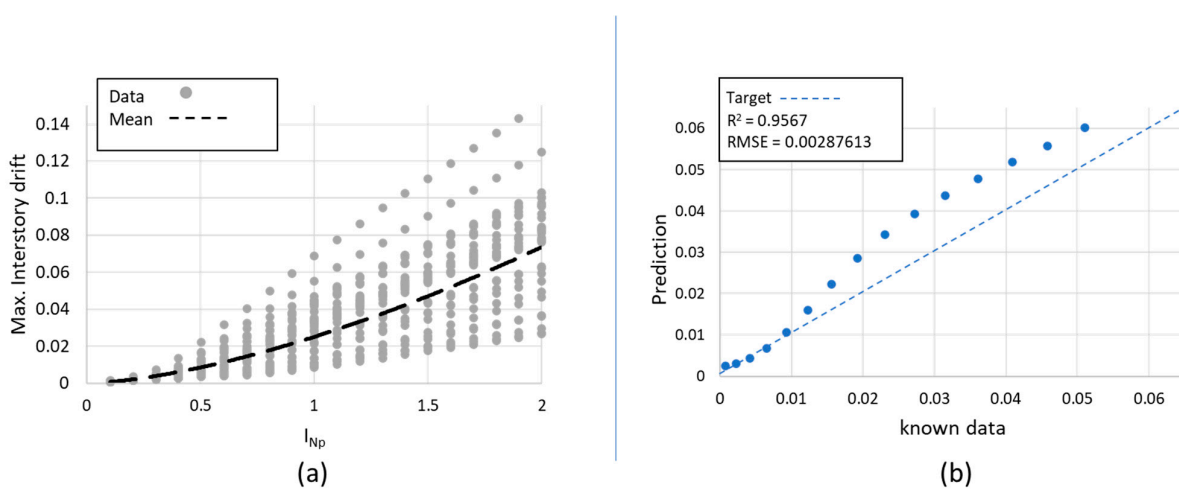**Figure 14.** 3D view of the nine-story reinforced concrete building with BRBs.

Figure 15. Seismic performance of the nine-story reinforced concrete building with BRBs: (**a**) Max. interstory drift and mean values via incremental dynamic analysis; (**b**) neural network predictions vs. mean values of the incremental dynamic analysis.

6. Seismic Performance Prediction of Nonlinear SDOF Structures via I_{Np} and Deep Learning

It is well known that the seismic performance of buildings is affected by many parameters like construction material, resisting system, etc. In the case of RC, BRBs frames, or most of the structural systems, the response prediction is very complicated, and the results can vary significantly. For this reason, all the seismic design codes around the world present earthquake-resistant methodologies, earthquake design spectra, record selection strategies for nonlinear dynamic analysis, ductility reduction factors, hazard analysis, and so on, based mainly on simplified models of the common, well-known single degree of freedom systems as the core of earthquake engineering. Motivated by this issue, thousands of nonlinear seismic analyses of various elastoplastic SDOF systems with different structural and in general dynamic characteristics (structural periods T, and seismic coefficients C_y), as those indicated in Figure 16, are obtained by using incremental dynamic analyses in terms of the novel and efficient intensity measure I_{Np}. Notice that, in this case, the new structural response parameters, ductility, and normalized hysteretic energy (the ratio of the hysteretic energy divided by the force and displacement at yielding), have been incorporated and calibrated via deep learning. These parameters have been selected since the ductility parameter is crucial in the international building codes; in fact, the ductility reduction factors usually selected to take into account the nonlinear behavior are based on the ductility [52–54]. The third parameter selected for this study was hysteretic energy, which is currently the most important parameter to account for cumulative demands on the structural design of buildings under earthquakes [55–57]. It is important to say that most of the new energy-based procedures and damage indices are based on hysteretic energy [58–63]. As an example, and for the sake of brevity, only the results of the incremental dynamic analyses of nonlinear systems with a period equal to one are presented for seismic coefficients of 0.2 and 0.3 in terms of ductility and in terms of normalized hysteretic energy demands, and for a period equal to two and for seismic coefficients of 0.2 and 0.3 (see Figures 17 and 18).
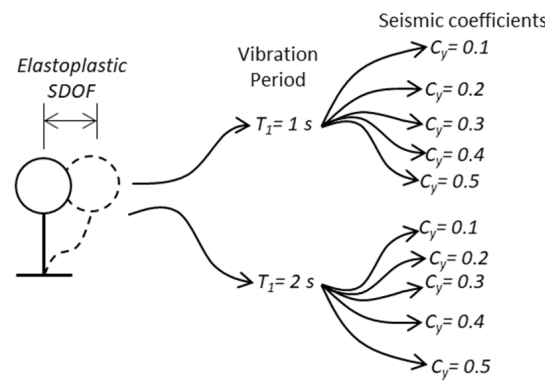

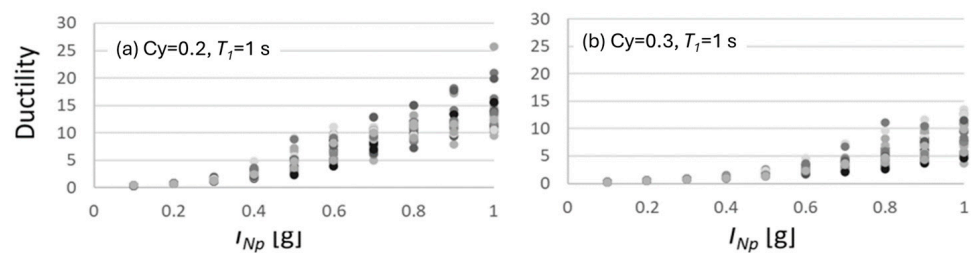**Figure 16.** Characteristics of the SDOF structural models.

Figure 17. Ductility demands obtained via incremental dynamic analysis.
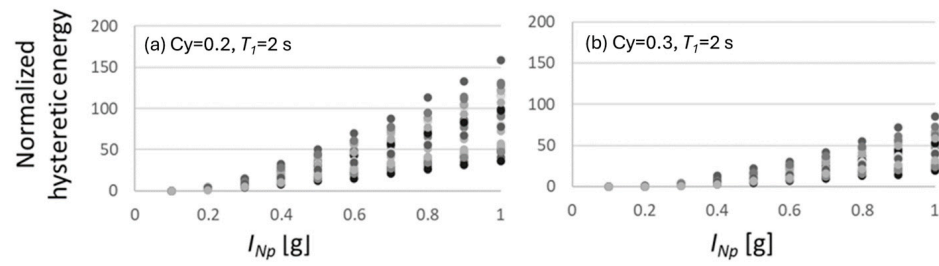
Figure 18. Normalized hysteretic energy demands obtained via incremental dynamic analysis.

To analyze the performance of the approach presented via deep learning to predict the new parameters, the results obtained for ductility and normalized hysteretic energy are presented below. Figure 19 shows the configuration adopted in terms of input and output layers. Due to the large increase in outputs, it has been considered to add an important input (seismic coefficient C_y, one of the key parameters for earthquake-resistant design of buildings) to properly relate the problem with the new output parameters.
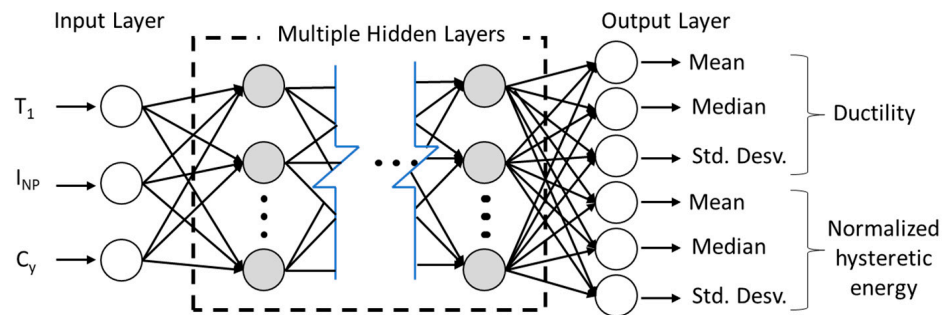

Figure 19. Deep neural networks to estimate the mean, median, and standard deviation of ductility and normalized hysteric energy.

Table 8 presents the results of the training process to predict statistics of ductility and normalized hysteretic energy. It can be observed that the error decreases as the depth of the neuronal network increases; nevertheless, from five hidden layers, the overfitting problem is noticeable because the difference between the training error and evaluation error begins to grow. In addition, the Taylor diagram shown in Figure 20 helps to visualize the behavior of the model prediction performance. In this case, a better correlation and accuracy is observed when using more hidden layers.
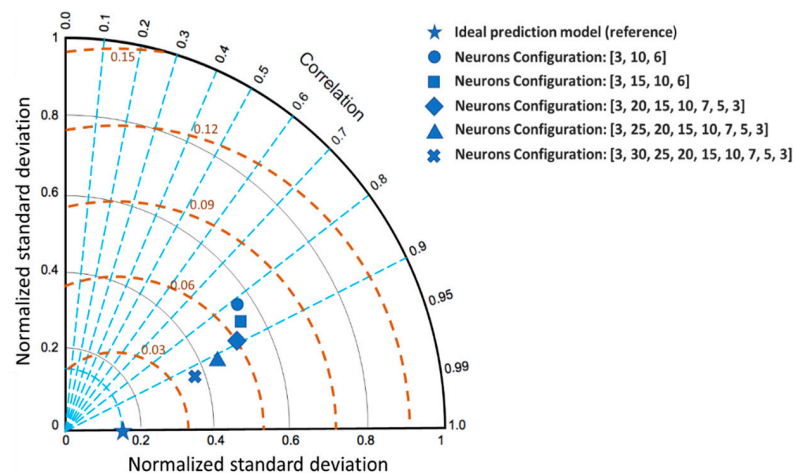

Figure 20. Taylor diagram of models to predict statistics of ductility and hysteretic energy.

Table 8. Results of training process to predict statistics of ductility and hysteretic energy.

Neurons Configuration	Hidden Layers	Evaluation Data	Training Iterations	MSE Training Data	R^2 Training Data	MSE Evaluation Data	R^2 Evaluation Data
[3, 6]	0	30%	5000	0.126	0.82	0.134	0.80
[3, 10, 6]	1	30%	5000	0.090	0.85	0.115	0.82
[3, 15, 10, 3]	2	30%	5000	0.085	0.87	0.097	0.83
[3, 20, 15, 10, 7, 5, 3]	3	30%	5000	0.068	0.89	0.090	0.85
[3, 25, 20, 15, 10, 7, 5, 3]	4	30%	5000	0.058	0.91	0.060	0.91
[3, 30, 25, 20, 15, 10, 7, 5, 3]	5	30%	5000	0.049	0.92	0.069	0.89

7. Conclusions

In this study, several RC structural frames were dynamically analyzed using ground motion records scaled at different values of the spectral acceleration $Sa(T_1)$ and the ground motion intensity measure I_{Np} to compute the maximum interstory drift. The maximum interstory drift obtained was summarized using the statistical parameters known as mean, median, and standard deviation. Computational models based on artificial neural networks with multi-hidden layers were designed to evaluate the degree of prediction of the seismic response. The fundamental period and the seismic intensity measurement were proposed as the only input neurons to predict the statistical parameters of the maximum interstory drift.

The analysis of the results obtained from the training process demonstrated that, by increasing the number of hidden layers, it is possible to solve the determination problem due to the multiple non-linear transformations required. With a configuration of two hidden layers, an acceptable degree of prediction was obtained for only one of the three output variables. The approach towards a deep network configuration improved the prediction of all three variables; however, from five hidden layers, the problem of overfitting was evidenced significantly.

A cross-validation analysis was developed to evaluate the independence of the magnitude of the prediction error in relation to the randomly selected data set in the neural network training and testing process. Furthermore, the performance of the predictive learning models was visually evaluated using a Taylor diagram. In conclusion, the computational model based on deep learning can predict the structural behavior of buildings under earthquake ground motions in terms of the maximum interstory drift demand with good accuracy, acceptable cross-validation, and very close to ideal performance. The results also show that neural networks are a very flexible tool because it is possible to increase the number of input variables for the consideration of other structural forms; nevertheless, given the results of the different training tests, a major increase in computational demand is anticipated, which could be the scope of another study.

With the RC structures analyzed, an RC-BRB framed building with nine stories is tested to validate the model presented. The results indicate that a coefficient of determination (R^2) of 95% was obtained in such a way that the deep neural network could be a good tool for seismic predesign tasks and the fast estimation of the structural response or performance of buildings under earthquakes.

Finally, because all the seismic design codes around the world are used to present earthquake-resistant approaches, design spectra, record selection strategies for seismic analysis, and so on, based mainly on simplified models as the commonly well-known single degree of freedom systems as the core of the earthquake engineering, thousands of seismic response analyses of several nonlinear elastoplastic SDOF systems were computed. These new numerical results provide the effectiveness of deep learning neural network models for structural prediction in terms of ductility and hysteretic energy demands of seismic performance. Therefore, this study is oriented toward the earthquake-resistant predesign and the fast estimation of the structural response of buildings under earthquakes using artificial intelligence advances in terms of the most important design parameters and by means of advanced and efficient intensity measures such as the novel I_{Np}.

For future research, analyzing the dataset using basic neural network architectures, including Feed Forward (FF), Radial Basis Function (RBF), and Multi-Layer Perceptron (MLP) models is planned, as well as comparing their performance against the deep learning and fast predesign techniques presented by other researchers.

Appendix A

Dataset of statistical parameters about maximum interstory drift.

Period of Vibration	I_{Np}	Mean	Std. Desv.	Median
0.9	0.1	0.00198557	0.00018930	0.00195350
0.9	0.2	0.00397103	0.00037838	0.00390650
0.9	0.3	0.00593630	0.00054159	0.00585900
0.9	0.4	0.00803373	0.00075550	0.00800800
0.9	0.5	0.01178300	0.00246631	0.01066000
0.9	0.6	0.02134267	0.01051187	0.01768500
0.9	0.7	0.03442300	0.01713227	0.03376500
0.9	0.8	0.04790433	0.02367704	0.04695000
0.9	0.9	0.06115533	0.02682896	0.05965500
0.9	1	0.07689667	0.03224495	0.07299000
0.9	1.1	0.09194733	0.03621639	0.09150000
0.9	1.2	0.10524233	0.03840779	0.10685000
0.9	1.3	0.12248200	0.04450585	0.11635000
0.9	1.4	0.13362267	0.04366843	0.13725000
0.9	1.5	0.15169600	0.04790769	0.15115000
1.2	0.1	0.00175870	0.00025072	0.00167250
1.2	0.2	0.00351747	0.00050132	0.00334550
1.2	0.3	0.00527587	0.00076145	0.00501850
1.2	0.4	0.00737523	0.00106450	0.00700900
1.2	0.5	0.01190380	0.00170633	0.01175000
1.2	0.6	0.02021367	0.00589694	0.01848500
1.2	0.7	0.02831367	0.00846909	0.02597000
1.2	0.8	0.03556167	0.00910376	0.03676500
1.2	0.9	0.04234233	0.00959351	0.04308000
1.2	1	0.04814133	0.01066981	0.04855000
1.2	1.1	0.05345333	0.01169260	0.05307000

Period of Vibration	I_{Np}	Mean	Std. Desv.	Median
1.2	1.2	0.05871833	0.01224732	0.05751000
1.2	1.3	0.06413967	0.01309662	0.06248500
1.2	1.4	0.07016600	0.01495424	0.06851000
1.2	1.5	0.07593100	0.01659735	0.07410000
1.38	0.1	0.00177580	0.00028973	0.00166350
1.38	0.2	0.00355183	0.00057954	0.00332750
1.38	0.3	0.00537903	0.00096485	0.00499100
1.38	0.4	0.00740917	0.00139175	0.00692350
1.38	0.5	0.01008277	0.00137013	0.00980850
1.38	0.6	0.01500067	0.00226893	0.01464000
1.38	0.7	0.02134900	0.00494191	0.02101000
1.38	0.8	0.02709833	0.00535109	0.02647500
1.38	0.9	0.03223300	0.00570592	0.03082000
1.38	1	0.03703900	0.00629038	0.03550000
1.38	1.1	0.04143833	0.00675983	0.03908000
1.38	1.2	0.04565000	0.00724887	0.04377500
1.38	1.3	0.04942667	0.00768099	0.04884500
1.38	1.4	0.05354900	0.00840227	0.05392500
1.38	1.5	0.05770500	0.00943261	0.05799000
1.53	0.1	0.00189230	0.00029065	0.00188800
1.53	0.2	0.00378440	0.00058139	0.00377600
1.53	0.3	0.00570843	0.00091909	0.00566400
1.53	0.4	0.00778640	0.00112739	0.00792050
1.53	0.5	0.01170440	0.00180979	0.01182500
1.53	0.6	0.01797733	0.00312006	0.01780000
1.53	0.7	0.02267433	0.00316726	0.02170000
1.53	0.8	0.02671800	0.00375887	0.02544500
1.53	0.9	0.03016967	0.00454644	0.02883500
1.53	1	0.03376000	0.00493950	0.03244500
1.53	1.1	0.03707567	0.00538001	0.03624500
1.53	1.2	0.04022967	0.00582309	0.03930000
1.53	1.3	0.04323533	0.00629872	0.04211000
1.53	1.4	0.04640567	0.00690343	0.04497500
1.53	1.5	0.04966700	0.00761394	0.04785500

References

1. Wieland, M. Safety Aspects of Sustainable Storage Dams and Earthquake Safety of Existing Dams. *Engineering* **2016**, *2*, 325–331. [CrossRef]
2. Rezvani Sharif, M.; Sadri Tabaei Zavareh, S.M.R. Predictive Modeling of the Lateral Drift Capacity of Circular Reinforced Concrete Columns Using an Evolutionary Algorithm. *Eng. Comput.* **2019**, *37*, 1579–1591. [CrossRef]
3. Takagi, J.; Wada, A. Higher Performance Seismic Structures for Advanced Cities and Societies. *Engineering* **2019**, *5*, 184–189. [CrossRef]
4. Fujino, Y.; Siringoringo, D.M.; Ikeda, Y.; Nagayama, T.; Mizutani, T. Research and Implementations of Structural Monitoring for Bridges and Buildings in Japan. *Engineering* **2019**, *5*, 1093–1119. [CrossRef]
5. Nishiyama, I.; Kuramoto, H.; Noguchi, H. Guidelines: Seismic Design of Composite Reinforced Concrete and Steel Buildings. *J. Struct. Eng.* **2004**, *130*, 336–342. [CrossRef]
6. Yang, H.; Feng, Y.; Wang, H.; Jeremić, B. Energy Dissipation Analysis for Inelastic Reinforced Concrete and Steel Beam-Columns. *Eng. Struct.* **2019**, *197*, 109431. [CrossRef]
7. Xiao, J.; Zhang, K.; Ding, T.; Zhang, Q.; Xiao, X. Fundamental Issues towards Unified Design Theory of Recycled and Natural Aggregate Concrete Components. *Engineering* **2023**, *29*, 188–197. [CrossRef]
8. Qiu, C.; Du, X.; Teng, J.; Li, Z.; Chen, C. Seismic Design Method for Multi-Story SMA Braced Frames Based on Inelastic Displacement Ratio. *Soil. Dyn. Earthq. Eng.* **2021**, *147*, 106794. [CrossRef]
9. Housner, G.W. Spectrum Intensities of Strong-Motion Earthquakes. In Proceedings of the Symposium on Earthquake and Blast Effects on Structures, Los Angeles, CA, USA, June 1952; EERI: Oakland, CA, USA, 1952.
10. Arias, A. A Measure of Earthquake Intensity. In *Seismic Design for Nuclear Power Plants*; MIT Press: Cambridge, MA, USA, 1970; ISBN 9780262080415.

11. Padgett, J.E.; Nielson, B.G.; DesRoches, R. Selection of Optimal Intensity Measures in Probabilistic Seismic Demand Models of Highway Bridge Portfolios. *Earthq. Eng. Struct. Dyn.* **2008**, *37*, 711–725. [CrossRef]
12. Kazantzi, A.K.; Vamvatsikos, D. Intensity Measure Selection for Vulnerability Studies of Building Classes. *Earthq. Eng. Struct. Dyn.* **2015**, *44*, 2677–2694. [CrossRef]
13. Bojórquez, E.; Baca, V.; Bojórquez, J.; Reyes-Salazar, A.; Chávez, R.; Barraza, M. A Simplified Procedure to Estimate Peak Drift Demands for Mid-Rise Steel and R/C Frames under Narrow-Band Motions in Terms of the Spectral-Shape-Based Intensity Measure I_{Np}. *Eng. Struct.* **2017**, *150*, 334–345. [CrossRef]
14. Torres, J.I.; Bojórquez, E.; Chavez, R.; Bojórquez, J.; Reyes-Salazar, A.; Baca, V.; Valenzuela, F.; Carvajal, J.; Payán, O.; Leal, M. Peak Floor Acceleration Prediction Using Spectral Shape: Comparison between Acceleration and Velocity. *Earthq. Struct.* **2021**, *21*, 551–562. [CrossRef]
15. Tothong, P.; Luco, N. Probabilistic Seismic Demand Analysis Using Advanced Ground Motion Intensity Measures. *Earthq. Eng. Struct. Dyn.* **2007**, *36*, 1837–1860. [CrossRef]
16. Mehanny, S.S.F. A Broad-Range Power-Law Form Scalar-Based Seismic Intensity Measure. *Eng. Struct.* **2009**, *31*, 1354–1368. [CrossRef]
17. Bojórquez, E.; Iervolino, I. Spectral Shape Proxies and Nonlinear Structural Response. *Soil. Dyn. Earthq. Eng.* **2011**, *31*, 996–1008. [CrossRef]
18. Buratti, N. A Comparison of the Performances of Various Ground–Motion Intensity Measures. In Proceedings of the 15th World Conference on Earthquake Engineering, Lisbon, Portugal, 24–28 September 2012.
19. Cai, J.; Bu, G.; Yang, C.; Chen, Q.; Zuo, Z. Calculation Methods for Inter-Story Drifts of Building Structures. *Adv. Struct. Eng.* **2014**, *17*, 735–745. [CrossRef]
20. Lee, H.J.; Aschheim, M.A.; Kuchma, D. Interstory Drift Estimates for Low-Rise Flexible Diaphragm Structures. *Eng. Struct.* **2007**, *29*, 1375–1397. [CrossRef]
21. Ruiz-García, J.; Miranda, E. Probabilistic Estimation of Residual Drift Demands for Seismic Assessment of Multi-Story Framed Buildings. *Eng. Struct.* **2010**, *32*, 11–20. [CrossRef]
22. VANLUCHENE, R.D.; SUN, R. Neural Networks in Structural Engineering. *Comput.-Aided Civ. Infrastruct. Eng.* **1990**, *5*, 207–215. [CrossRef]
23. Adeli, H. Neural Networks in Civil Engineering: 1989–2000. *Comput.-Aided Civ. Infrastruct. Eng.* **2001**, *16*, 126–142. [CrossRef]
24. Rafiq, M.Y.; Bugmann, G.; Easterbrook, D.J. Neural Network Design for Engineering Applications. *Comput. Struct.* **2001**, *79*, 1541–1552. [CrossRef]
25. Barraza, M.; Bojórquez, E.; Fernández-González, E.; Reyes-Salazar, A. Multi-Objective Optimization of Structural Steel Buildings under Earthquake Loads Using NSGA-II and PSO. *KSCE J. Civ. Eng.* **2017**, *21*, 488–500. [CrossRef]
26. Leyva, H.; Bojórquez, J.; Bojórquez, E.; Reyes-Salazar, A.; Carrillo, J.; López-Almansa, F. Multi-Objective Seismic Design of BRBs-Reinforced Concrete Buildings Using Genetic Algorithms. *Struct. Multidiscip. Optim.* **2021**, *64*, 2097–2112. [CrossRef]
27. Reyes, H.E.; Bojórquez, J.; Cruz-Reyes, L.; Ruiz, S.E.; Reyes-Salazar, A.; Bojórquez, E.; Barraza, M.; Formisano, A.; Payán, O.; Torres, J.R. Development an Artificial Neural Network Model for Estimating Cost of R/C Building by Using Life-Cycle Cost Function: Case Study of Mexico City. *Adv. Civ. Eng.* **2022**, *2022*, 7418230. [CrossRef]
28. Zhou, Y.; Meng, S.; Lou, Y.; Kong, Q. Physics-Informed Deep Learning-Based Real-Time Structural Response Prediction Method. *Engineering* **2024**, *35*, 140–157. [CrossRef]
29. Marcelin, J.L. Evolutionary Optimisation of Mechanical Structures: Towards an Integrated Optimisation. *Eng. Comput.* **1999**, *15*, 326–333. [CrossRef]
30. Spencer, B.F.; Hoskere, V.; Narazaki, Y. Advances in Computer Vision-Based Civil Infrastructure Inspection and Monitoring. *Engineering* **2019**, *5*, 199–222. [CrossRef]
31. Rao, M.A.; Srinivas, J. Torsional Vibrations of Pre-Twisted Blades Using Artificial Neural Network Technology. *Eng. Comput.* **2000**, *16*, 10–15. [CrossRef]
32. Lecun, Y.; Bengio, Y.; Hinton, G. Deep Learning. *Nature* **2015**, *521*, 436–444. [CrossRef]
33. Seo, J.; Kapania, R.K. Topology Optimization with Advanced CNN Using Mapped Physics-Based Data. *Struct. Multidiscip. Optim.* **2023**, *66*, 21. [CrossRef]
34. Mohammed Sahib, M.; Kovács, G. Multi-Objective Optimization of Composite Sandwich Structures Using Artificial Neural Networks and Genetic Algorithm. *Results Eng.* **2024**, *21*, 101937. [CrossRef]
35. Kim, K.G. Book Review: Deep Learning. *Health Inf. Res.* **2016**, *22*, 351–354. [CrossRef]
36. Harrou, F.; Dairi, A.; Dorbane, A.; Sun, Y. Energy Consumption Prediction in Water Treatment Plants Using Deep Learning with Data Augmentation. *Results Eng.* **2023**, *20*, 101428. [CrossRef]
37. Armghan, A.; Logeshwaran, J.; Sutharshan, S.M.; Aliqab, K.; Alsharari, M.; Patel, S.K. Design of Biosensor for Synchronized Identification of Diabetes Using Deep Learning. *Results Eng.* **2023**, *20*, 101382. [CrossRef]
38. Payán-Serrano, O.; Bojórquez, E.; Bojórquez, J.; Chávez, R.; Reyes-Salazar, A.; Barraza, M.; López-Barraza, A.; Rodríguez-Lozoya, H.; Corona, E. Prediction of Maximum Story Drift of MDOF Structures under Simulated Wind Loads Using Artificial Neural Networks. *Appl. Sci.* **2017**, *7*, 563. [CrossRef]
39. Morfidis, K.; Kostinakis, K. Approaches to the rapid seismic damage prediction of r/c buildings using artificial neural networks. *Eng. Struct.* **2018**, *165*, 120–141. [CrossRef]

40. Mishra, M.; Bhatia, A.S.; Maity, D. A Comparative Study of Regression, Neural Network and Neuro-Fuzzy Inference System for Determining the Compressive Strength of Brick–Mortar Masonry by Fusing Nondestructive Testing Data. *Eng. Comput.* **2019**, *37*, 77–91. [CrossRef]

41. Raza, A.; Adnan Raheel Shah, S.; ul Haq, F.; Arshad, H.; Safdar Raza, S.; Farhan, M.; Waseem, M. Prediction of Axial Load-Carrying Capacity of GFRP-Reinforced Concrete Columns through Artificial Neural Networks. *Structures* **2020**, *28*, 1557–1571. [CrossRef]

42. Yuan, X.; Zhong, J.; Zhu, Y.; Chen, G.; Dagli, C. Post-earthquake regional structural damage evaluation based on artificial neural networks considering variant structural properties. *Structures* **2023**, *52*, 971–982. [CrossRef]

43. Hassoun, M.H. *Fundamentals of Artificial Neural Networks*; The MIT Press: Cambridge, MA, USA, 2005. [CrossRef]

44. Yegnanarayana, B. Artificial Neural Networks for Pattern Recognition. *Sadhana* **1994**, *19*, 189–238. [CrossRef]

45. Morelli, M.; Hauth, J.; Guardone, A.; Huan, X.; Zhou, B.Y. A Rotorcraft In-Flight Ice Detection Framework Using Computational Aeroacoustics and Bayesian Neural Networks. *Struct. Multidiscip. Optim.* **2023**, *66*, 197. [CrossRef]

46. Vamvatsikos, D.; Allin Cornell, C. Incremental Dynamic Analysis. *Earthq. Eng. Struct. Dyn.* **2002**, *31*, 491–514. [CrossRef]

47. Kingma, D.P.; Ba, J.L. Adam: A Method for Stochastic Optimization. In Proceedings of the 3rd International Conference on Learning Representations, ICLR 2015—Conference Track Proceedings, San Diego, CA, USA, 7–9 May 2015.

48. Panchal, G.; Ganatra, A.; Shah, P.; Panchal, D. Determination of Over-Learning and Over-Fitting Problem in Back Propagation Neurl Network. *Int. J. Soft Comput.* **2011**, *2*, 40–51. [CrossRef]

49. Koziel, S.; Calik, N.; Mahouti, P.; Belen, M. Accurate Modeling of Antenna Structures by Means of Domain Confinement and Pyramidal Deep Neural Networks. *IEEE Trans. Antennas Propag.* **2022**, *70*, 2174–2188. [CrossRef]

50. Browne, M.W. Cross-Validation Methods. *J. Math. Psychol.* **2000**, *44*, 108–132. [CrossRef] [PubMed]

51. Dabiri, H.; Rahimzadeh, K.; Kheyroddin, A. A Comparison of Machine Learning- and Regression-Based Models for Predicting Ductility Ratio of RC Beam-Column Joints. *Structures* **2022**, *37*, 69–81. [CrossRef]

52. Park, R. Evaluation of Ductility of Structures and Structural Assemblages from Laboratory Testing. *Bull. New Zealand Soc. Earthq. Eng.* **1989**, *22*, 155–166. [CrossRef]

53. Moghaddam, H.; Mohammadi, R.K. Ductility Reduction Factor of MDOF Shear-Building Structures. *J. Earthq. Eng.* **2001**, *5*, 425–440. [CrossRef]

54. Arslan, M.H. Estimation of Curvature and Displacement Ductility in Reinforced Concrete Buildings. *KSCE J. Civ. Eng.* **2012**, *16*, 759–770. [CrossRef]

55. Kunnath, S.K.; Chai, Y.H. Cumulative Damage-Based Inelastic Cyclic Demand Spectrum. *Earthq. Eng. Struct. Dyn.* **2004**, *33*, 499–520. [CrossRef]

56. Bojórquez, E.; Terán-Gilmore, A.; Ruiz, S.E.; Reyes-Salazar, A. Evaluation of Structural Reliability of Steel Frames: Interstory Drift versus Plastic Hysteretic Energy. *Earthq. Spectra* **2011**, *27*, 661–682. [CrossRef]

57. Zhou, Y.; Song, G.; Tan, P. Hysteretic Energy Demand for Self-Centering SDOF Systems. *Soil. Dyn. Earthq. Eng.* **2019**, *125*, 105703. [CrossRef]

58. Bojorquez, E.; Ruiz, S.E.; Teran-Gilmore, A. Reliability-Based Evaluation of Steel Structures Using Energy Concepts. *Eng. Struct.* **2008**, *30*, 1745–1759. [CrossRef]

59. Bojórquez, E.; Reyes-Salazar, A.; Terán-Gilmore, A.; Ruiz, S.E. Energy-Based Damage Index for Steel Structures. *Steel Compos. Struct.* **2010**, *10*, 331–348. [CrossRef]

60. Song, Z.; Konietzky, H.; Frühwirt, T. Hysteresis Energy-Based Failure Indicators for Concrete and Brittle Rocks under the Condition of Fatigue Loading. *Int. J. Fatigue* **2018**, *114*, 298–310. [CrossRef]

61. Qiu, C.; Qi, J.; Chen, C. Energy-Based Seismic Design Methodology of SMABFs Using Hysteretic Energy Spectrum. *J. Struct. Eng.* **2020**, *146*, 04019207. [CrossRef]

62. Gentile, R.; Galasso, C. Hysteretic Energy-based State-dependent Fragility for Ground-motion Sequences. *Earthq. Eng. Struct. Dyn.* **2021**, *50*, 1187–1203. [CrossRef]

63. Gholami, N.; Garivani, S.; Askariani, S.S.; Hajirasouliha, I. Estimation of Hysteretic Energy Distribution for Energy-Based Design of Structures Equipped with Dampers. *J. Build. Eng.* **2022**, *51*, 104221. [CrossRef]